AIAA AVIATION Forum
June 27-July 1, 2022, Chicago, IL & Virtual
AIAA AVIATION 2022 Forum

10.2514/6.2022-3897

Prediction of Vortex Initiation using an Unsteady Panel Method with an Integral-Boundary-Layer Calculation

Hariharan Ramanathan,* and Ashok Gopalarathnam†
Department of Mechanical and Aerospace Engineering, North Carolina State University, Raleigh, NC, 27695

In our current work, we implement and evaluate the efficacy of a boundary layer parameter (H_{32}) based low-order model to signal the onset of leading-edge vortex (LEV) initiation for low Re flows ($O(10^4)$) . In an earlier work(AIAA Aviation Forum 2019, p.3590) using numerical simulations, it was proven that the shape factor parameter (H_{32}) attains a critical value of ~ 1.52 prior to the formation of dynamic stall vortex (DSV) irrespective of airfoil, motion kinematics. Numerical simulations spanned high pitch rate motions ($K \geq 0.1$) and three leading edge radii ($0.5 \leq r_{LE} \leq 2.0$) for three different pivot locations : leading-edge (LE), quarter-chord (QC) and half-chord (HC). This finding concurred with the H_{32} value reported in literature for laminar separation (H_{32} = 1.515) in steady incompressible flows. In the second part of the effort, we focus on low-order prediction of LEV initiation using this criticality. This was achieved using an inviscid calculation of unsteady-airfoil velocity and pressure distributions, which serve as an input to a quasi-steady integral boundary layer (IBL) method. The results provided here demonstrate the effectiveness of H_{32} in predicting leading-edge flow reversal. We show, by analysing different cases, that this inexpensive method has crucial ramifications in picking the appropriate $LESP_{crit}$ for any given airfoil and motion combination. Hence, we eliminate the need for CFD, Experiments to obtain $LESP_{crit}$ for a new parameter set.

Nomenclature

α	= angle of attack, deg
$\dot{\alpha}$	= rate of change of angle of attack, rad/sec
α_{crit}	= critical angle of attack, deg
U_∞	= freestream velocity, m/s
c	= airfoil chord, m
t	= time, s
C_f	= skin-friction coefficient
$_{LE}$	= leading edge radius of airfoil
δ_2	= momentum thickness
δ_3	= energy thickness
H_{32}	= Shape factor $\frac{\delta_3}{\delta_2}$
t^*	= non-dimensional time, tU_∞/c
γ	= Bound vorticity, m/s
Γ	= Wake vorticity, m^2/s
Φ	= Velocity Potential, m^2/s
Re	= Reynolds number based on c
K	= reduced pitch rate, $\dot{\alpha}c/2U_\infty$
$LESP$	= leading edge suction parameter
$LESP_{crit}$	= critical value of $LESP$
C_l	= lift coefficient
C_d	= drag coefficient

*Ph.D. Candidate, Department of Mechanical and Aerospace Engineering, Student Member, AIAA
†Professor, Department of Mechanical and Aerospace Engineering, Associate Fellow, AIAA

I. Introduction

Unsteady flow phenomenon especially dynamic stall has been receiving significant attention in recent years. This nonlinear phenomenon is attributed to either time varying movements of the wing or sudden changes in freestream conditions. The applications extend to bio-inspired flight [1], helicopter rotors (Ham and Garelick [2]) and flapping foil energy harvesters (Su and Breuer [3]). The formation of a leading-edge vortex (LEV) plays a key role in these scenarios demonstrating an interrelation between forces and motion kinematics. This long standing interest in the study of LEV formation has led researchers to formulate various tools to predict the onset of dynamic stall. Early work by Evans and Mort [4] showed the correlation between maximum leading-edge suction and subsequent LEV formation. Baik et al. [5] have studied the influence of leading-edge vortices in detail using experimental methods. In recent times, discrete vortex methods based low-order models (Ramesh et al. [6]) and phenomenological models (Wang and Eldredge [7]) have been preferred for real-time rapid prediction. Amongst these, the LESP - modulated discrete vortex method (LDVM) developed by Ramesh et al. [6] has been universally accepted as a reliable criterion to predict LEV shedding. The novelty with LESP lies in its consistency irrespective of change in motion kinematics and being solely dependant on Reynolds number (Re) and leading-edge radii (r_{LE}). In order to extend the applicability of LESP over a wider range of pitch rates (K) and Reynolds numbers (Re), Narsipur et al. [8] updated the LESP formulation taking into account the high motion-induced velocities (higher K) along with the freestream terming it as $LESP_{net}$. Though the efforts reduced the sensitivity of LESP for high Re flows and high K motions, application of this insight for a new airfoil and Reynolds number combination still relies on the support of high order methods (CFD or Experiments) to obtain the $LESP_{net}$ for that r_{LE} and Re combination. In the current work, we study a large set of computational results from unsteady Reynolds-averaged Navier-Stokes (RANS) simulations of pitching aerofoils, identify a novel boundary layer parameter and implement this in a low cost computational tool to predict the first occurrence of leading-edge flow reversal. We aim to use the criticality of a boundary layer parameter and hence improve on the $LESP_{net}$ predictions for a given airfoil, Re combination.

Though the process of the evolution of DSV and its convection has been long studied and documented in a myriad of studies like (Carr et al. [9], McCroskey [10]), what still poses as a challenge is delineating the occurrence of unsteady flow separation. The concept of vanishing shear stress being classified as separation by Prandtl [11] works extremely well with steady flows due to the separation point being fixed. Unlike the process of LEV initiation which can be assessed by monitoring the maximum leading-edge suction, the problem of characterizing unsteady flow separation is exacerbated by fluctuations in the movement of separation point which may not overlap with the zero skin-friction location as pointed out in previous works (Haller [12], Klose et al. [13]). The singularities encountered in tackling unsteady separation via a numerical approach prompt us to look elsewhere for a solution to address this transient phenomenon. We focussed on some underlying mechanisms playing a dominant role in the development of boundary layer around the leading-edge and came across multiple studies (Acharya and Metwally [14], Gehlert and Babinsky [15]) heralding the contribution of vorticity in such scenarios.

All these studies point towards the possibility of an intrinsic connection between the boundary layer criticality and initiation. Gendrich [16] suggests the definition of an unsteady separation point on the basis of the boundary layer thickness (δ), displacement thickness (δ^*) or momentum thickness (θ) relative to their initial values. Smith and Jones [17] proposed a Falkner-Skan parameter (β) as a criterion for LEV shedding. We take note of the fact that a quantity that is often associated with separation (in steady laminar flows at least) is the shape factor, $H = \frac{\delta^*}{\theta}$. For the zero pressure gradient (ZPG) flow over a flat plate, this value turns out to be 2.59 (Schlichting and Gersten [18]), when the flow is well-developed. Similarly for a certain class of velocity profiles, the value of H at separation shows consistency in both laminar (Erturk et al. [19]) and turbulent flows (Castillo et al. [20]). The authors in a previous effort [21] analysed the boundary layer behavior using numerical simulations and concluded the existence of a criticality in shape factor at the onset of initiation. In this paper, we implement this idea in a low-order model which would eventually indicate the appropriate $LESP_{net}$ to pick for a given combination of r_{LE} and Re.

In the upcoming sections, a brief background of the LESP concept is presented in §A. The next section (§III) briefly describes the computational set-up (§A), presents validation of the CFD between fully turbulent and laminar solutions for the same Re (§B). Subsequently, details of the boundary layer extraction (§C), unsteady vortex panel method (§D) and the integral boundary layer method (§E) are provided along with some results validation of the panel method with experiments and CFD (§1). In (§F), we list the cases of the unsteady motions studied in this work. The criterion used in identifying LEV initiation is described in §G. Using the methodology of boundary layer extraction, we analyse CFD results (§H) for the baseline case (Case 6) and apply this insight to develop a low-order model. This low-order model is then shown in (§IV) to be successful in predicting the LESP at the first instance of flow reversal. In the final section (§V), we present some conclusions from the current efforts.

II. Background

A. Leading-edge suction

Recent progress by Ramesh et al. [6] in the development of a criterion for LEV initiation on unsteady airfoils has provided the impetus for the current work. In that work, it was shown that, for unsteady airfoils undergoing high-rate motions, the initiation of LEV formation occurs when the instantaneous value of the leading-edge suction parameter, LESP, reaches a critical value,termed LESP$_{crit}$. The instantaneous LESP, which is a non-dimensional parameter that can be calculated in unsteady thin-airfoil theory, provides a measure of the aerodynamic condition at the leading edge (i.e., flow velocity, suction peak, and the adverse pressure gradient). It was shown that, so long as the motions considered do not result in significant trailing-edge reversed flow preceding the LEV formation, the LESP$_{crit}$ depends only on airfoil shape and Reynolds number, and is largely independent of motion kinematics. Thus, if LESP$_{crit}$ is determined from two-dimensional experiment or CFD for one high-rate motion, it can be used for low-order prediction of LEV initiation for any other high-rate motion. Using this insight, a low-order prediction method, named LESP-modulated discrete vortex method, or LDVM, was developed.

The following subsection briefly describes the LESP criterion for initiation of LEV formation on airfoils. The interested reader may refer to Ramesh et al. [6] for further details.

B. Criticality of LESP and LEV shedding on airfoils

It has been known for several decades that the onset of separation at the leading edge is governed by criticality of flow parameters at the leading edge. Several researchers [4, 22] have correlated leading-edge flow criticality to onset of leading-edge separation and/or static/dynamic stall. The LESP idea of Ramesh et al. [6], inspired in part by these works, was the result of the search for an appropriate parameter that could be determined as a part of an unsteady airfoil theoretical calculation.

The LESP is a measure of the suction at the leading edge, which in turn is caused by the stagnation point moving away from the leading edge when the airfoil is at an angle of attack. Ramesh et al. observed that the determining factor for the leading-edge suction for an airfoil is the circulation at the leading edge, $\gamma(0,t)$, which is represented by the first coefficient $A_0(t)$. The instantaneous LESP at any time instant is therefore taken as the value of $A_0(t)$ at that time as follows:

$$LESP(t) = A_0(t) \tag{1}$$

As noted by Katz [23], airfoils having rounded leading edges can support some suction even when the stagnation point is away from the airfoil leading edge. The amount of suction that can be supported is a characteristic of the airfoil shape and Reynolds number of operation. When these quantities are constant, it was shown in Ramesh et al. [6] that initiation of LEV formation always occurred at the same value of LESP regardless of motion kinematics and history, provided the LEV formation was not preceded by significant trailing-edge separation. This threshold value of LESP, which is a function of the airfoil shape and Reynolds number, is termed the critical LESP, or LESP$_{crit}$. This value of LESP$_{crit}$, for any given airfoil and Reynolds number, can be obtained from CFD or experimental predictions for a single motion [6], and can then be used for any other motion to predict LEV formation. In Ramesh et al. [6], this idea was used not only to predict initiation of LEV formation but also to predict subsequent vortex shedding from the leading edge and termination of LEV shedding. The LDVM code handles these events by using discrete-vortex shedding from the leading edge modulated by the difference between the instantaneous value of the LESP at any given time and the critical value.

III. Methodology

A. CFD

NCSU's REACTMB-INS[24, 25] solver is used for the computational fluid dynamics (CFD) calculations performed in this study. The governing equations are written in arbitrary Lagrangian/Eulerian form, which enables the motion of a body-fitted computational mesh in accord with prescribed rate laws. An incompressible version of Edwards' Low-Diffusion Flux Splitting Scheme (LDFSS) [26] is used for discretizing inviscid fluxes in space. Discretization of viscous terms is performed using a second-order central difference method. The LDFSS method is extended to higher order of accuracy in space using the Piecewise-Parabolic Method (PPM) [27]. For time integration, second-order temporal accuracy is achieved by using an implicit artificial compressibility method [26] with eight subiterations at each physical time step for continuity-equation convergence. A version of Spalart-Allmaras one-equation eddy-viscosity model, modified by Edwards and Chandra [28], is used for turbulence closure.

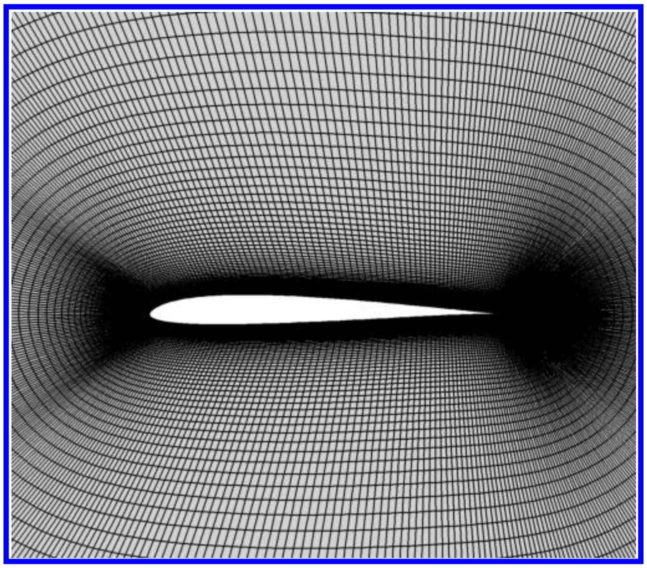

Fig. 1. Mesh topology around the airfoil

Figure 1 shows the representative mesh distribution used in the current work. In the current study, only SD7003 airfoil has been used as shown in Figure 9. The selected computational domain is a typical O-type grid, with its outer boundary 15 chords away from the airfoil, and structured grids are used for the whole domain. The distance of the first nodes adjacent to the airfoil surface is small enough so that the condition of $y^+ < 1$ is strictly guaranteed. Verification results for flow over a pitching airfoil are included and discussed in the following subsection.

B. CFD validation

Lee and Gerontakos [29] experimentally investigated the unsteady boundary layer and stall events occurring on a sinusoidally pitching NACA 0012 airfoil at $Re = 1.35 \times 10^5$. The article provides the force coefficients (C_l and C_d) for a given cycle. The measurements are used here to compare with REACTMB-INS predictions as shown in figure 2. Favourable agreement is observed between the measured data, and the REACTMB predictions.

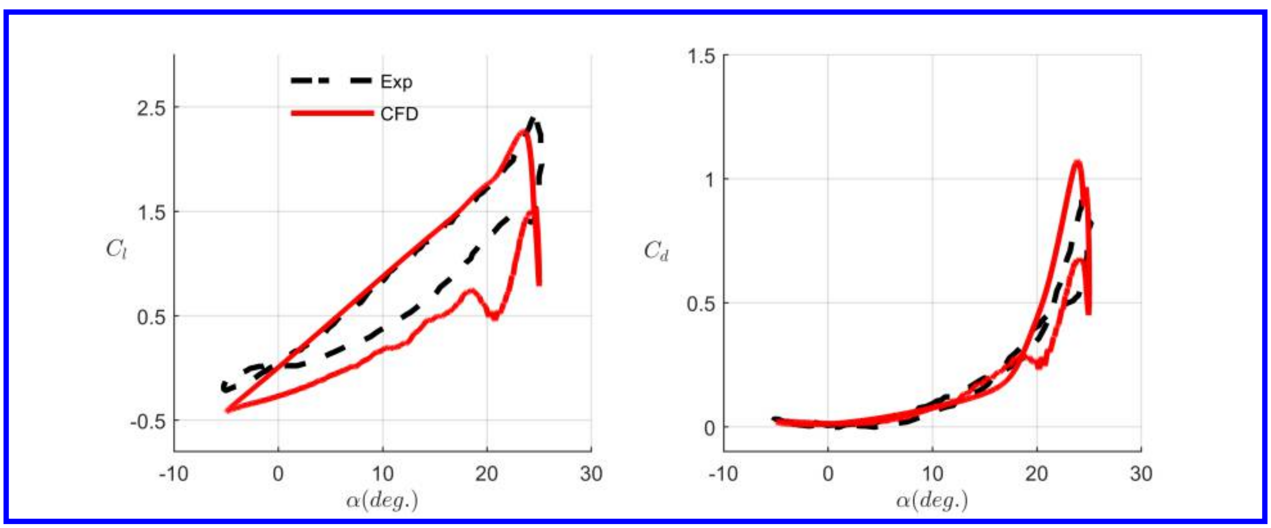

Fig. 2. Comparison for a sinusoidal pitching airfoil: computed C_l and C_d vs α compared with experimental results of [29] for the NACA 0012 airfoil at $Re = 1.35 \times 10^5$, $k = 0.10$, $\alpha(t) = 10 + 15\sin(\Omega t)$

The current study is focused on a low Reynolds number of 10,000. At these Reynolds numbers, it is known that the boundary layer is mostly laminar over the airfoil and especially at the leading edge. To explore the difference between using a the laminar flow CFD solution vs. using a Reynolds-averaged Navier Stokes (RANS) model, the REACTMB-INS code was used with both these options for the analysis of a SD7003 airfoil undergoing a pitch-up hold motion. analysis. The Spalart-Allmaras (SA) turbulence model was used for the RANS simulation. Figure 3 shows the results for C_l and C_d vs. convective time, t^*, from the two simulations. It is seen that the results are essentially identical. An examination of the flow field from the RANS simulation confirmed that, for this Reynolds number, the solver did not activate the turbulence model except in the wake behind the airfoil. Based on this analysis, it is seen that the airfoil flow, especially at the leading edge, is essentially laminar, and that the choice of laminar vs. RANS option in the CFD analysis does not matter for this condition. All the simulations in this paper are carried out using the RANS model with the SA turbulence model.

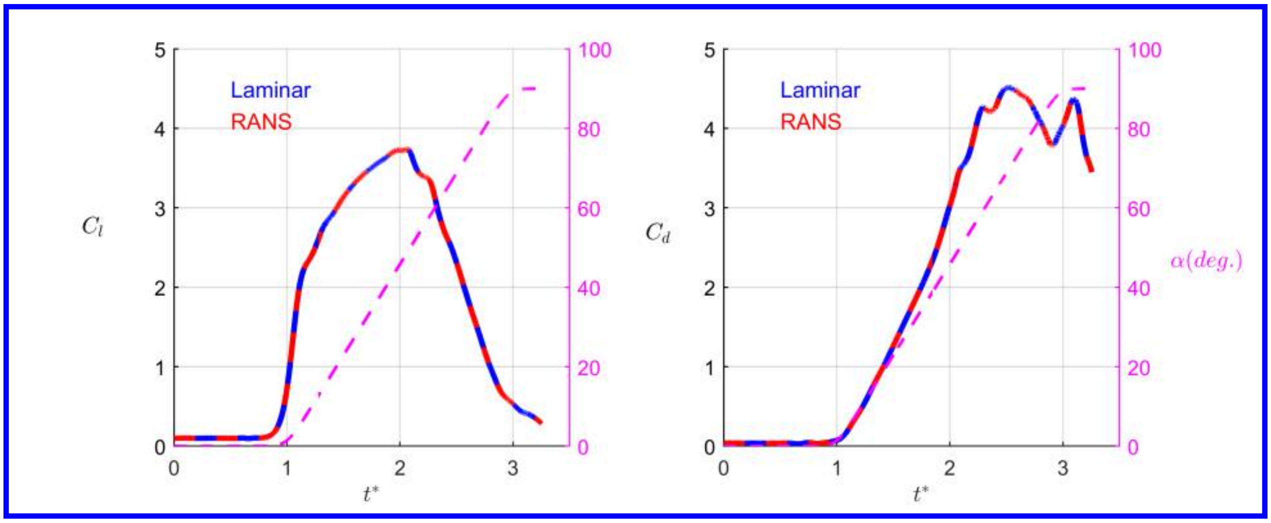

Fig. 3. Comparison for a pitch-up and hold airfoil: computed C_l and C_d vs α between laminar and fully turbulent flow results for the SD7003 airfoil at $Re = 1.0 \times 10^4$, $K = 0.4$

C. Boundary-layer extraction

In this method, we extract boundary-layer information from URANS computations for a large number of unsteady motions in the vicinity of leading edge. Critical locations in the flow field, i.e. stagnation point, onset of flow reversal, reattachment location and trailing edge separation, are identified to calculate $H_{32} = \frac{\delta_3}{\delta_2}$ at these locations. The edge of the boundary layer is typically determined using a mix of both vorticity and tangential velocity criteria. In the first step, we discretise the airfoil surface into panels and interpolate field data along the normal direction to each panel. In the current work, we have 50000 points along each normal as shown in Figure 4.

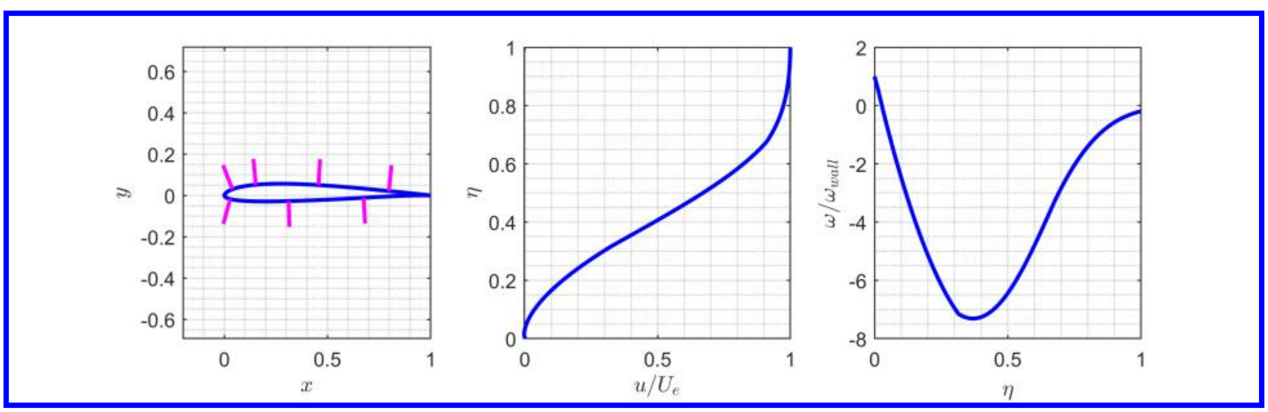

Fig. 4. (a) Probe locations. (b) Velocity profile within the boundary layer. (c) ω/ω_{wall}

Along each normal, we examine the vorticity ratio variation and identify a location which fits the criterion $\omega/\omega_{wall} < 10^{-5}$. Then, we identify ω_{max} on the airfoil and identify the location by tracking ω/ω_{max} along the normal in the opposite direction. In the last step, we check for the existence of a maximum in the velocity profile and choose that as the estimated boundary layer edge for that location. This study is repeated for different pitch rates to gauge the behaviour of H_{32} for different airfoils.

D. Unsteady Vortex Panel Method (UVPM)

Panel methods have been used in the past to analyze flow past bodies of realistic geometries and have proved to be successful under certain circumstances. It is important to understand that these methods are based on potential flow solutions and hence their forte lies in accurately solving attached flow fields. The use of these dates back to Hess and Smith [30]. Several extensions of these have been developed for many flow situations. In the current method, we extend this to unsteady motions.

In this UVPM, we use a linearly varying distribution of vorticity strength on each panel to model the bound vorticity (γ) and discrete trailing edge vortices(TEV) to model the wake vorticity (Γ) . TEVs are shed at every time step to satisfy Kelvin's condition ($\mathrm{d}\Gamma/\mathrm{d}t = 0$). The bound vorticity strength (γ_i) at each panel is determined by solving a matrix system of equations by imposing the flow tangency boundary condition at each panel ($\partial\Phi/\partial n = 0$) and enforcing the Kutta condition at the trailing edge ($\gamma_1 + \gamma_N = 0$). The expressions for velocity induced by a linearly varying vortex element in the panel coordinates are used from Katz and Plotkin [31].

For an airfoil with N panels and N-1 collocation points, the system of equations is given by:

$$\underbrace{\begin{bmatrix} a_{11} & a_{12} & \dots & a_{1N} & a_{1w} \\ a_{21} & a_{22} & \dots & a_{2N} & a_{2w} \\ \vdots & \vdots & \vdots & \vdots & \vdots \\ 1 & 0 & \dots & 1 & 0 \\ 0.5 * ds_1 & 0.5 * (ds_1 + ds_2) & \dots & 0.5 * ds_{N-1} & 1 \end{bmatrix}}_{\textbf{IC}} \underbrace{\begin{bmatrix} \gamma_1 \\ \gamma_2 \\ \vdots \\ \gamma_N \\ \Gamma_{wake} \end{bmatrix}}_{\gamma} \approx \underbrace{\begin{bmatrix} RHS_1 \\ RHS_2 \\ \vdots \\ 0 \\ \Gamma(t - \Delta t) \end{bmatrix}}_{\textbf{RHS}}$$

where *'ds'* refers to the length of each panel. The last column in influence coefficient (IC) matrix needs to be updated at the start of each time step depending on the location of the latest shed wake vortex. The discrete vortex core radius and placement methodology for the latest shed vortex is similar to that of [6].

Once velocities are obtained at the collocation points, the next step is to compute the pressure distribution around the airfoil. Unlike the steady scenario, it is imperative here that the velocity potential (Φ) be computed at every time step owing to finite $\partial\Phi/\partial t$. Using the unsteady Bernoulli equation $\frac{p_{\text{ref}} - p}{\rho} = \frac{V_t^2}{2} - \frac{v_{\text{kin}}^2}{2} + \frac{\partial\Phi}{\partial t}$ (V_t refers to the velocities at the collocation point, v_{kin} refers to the velocities due to motion kinematics), we can obtain the pressures at all panels and hence compute C_p.

1. Validation of UVPM

Three sets of comparisons were performed to establish the accuracy of the unsteady vortex panel method. In the first set of comparisons, we looked at experimental results from [32] for a sinusoidal pitching NACA 0018 airfoil at a freestream Reynolds number (Re) of 0.37 million. The computed coefficient of pressure (C_p) shows great agreement with experimental results as shown in Figure 5.

In the next set of comparisons, we also compared the velocity distributions between UVPM and CFD results for an SD7003 airfoil from the current work. Figures 6 and 7 display an excellent agreement with CFD results. Similar to C_p plots, the velocity distribution in suction region are higher in UVPM due to the absence of viscous effects.

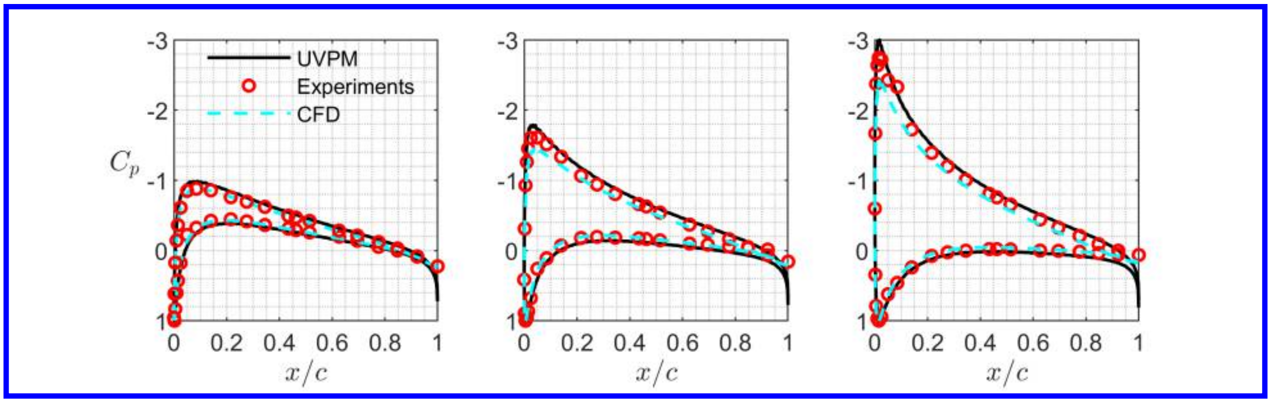

Fig. 5. C_p **comparisons between UVPM, experimental data (L-R) (a)** α = 2.1° **(b)** α = 5.9° **(c)** α = 9.3°

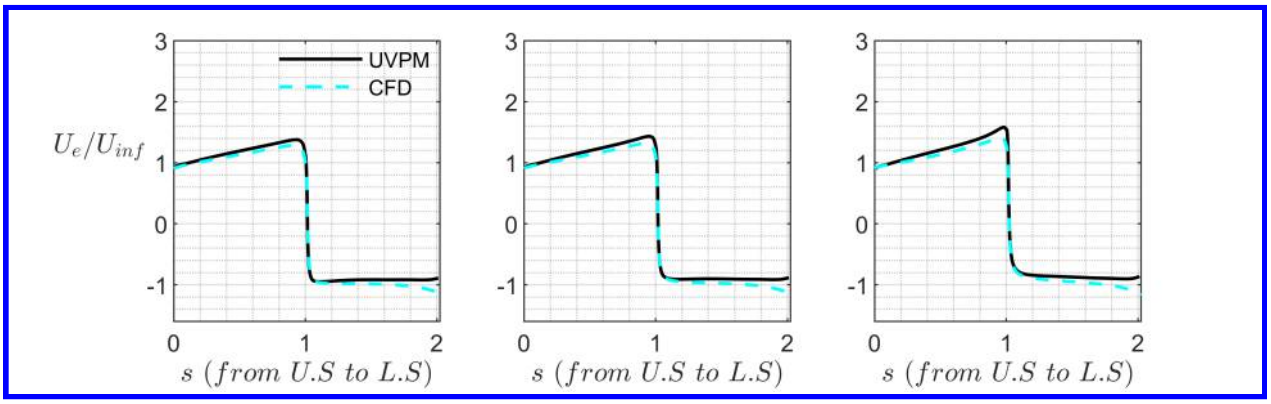

Fig. 6. Velocity distributions for K = 0.1, half-chord pivot (L-R) (a) α = 6.3° **(b)** α = 7.45° **(c)** α = 9.74°

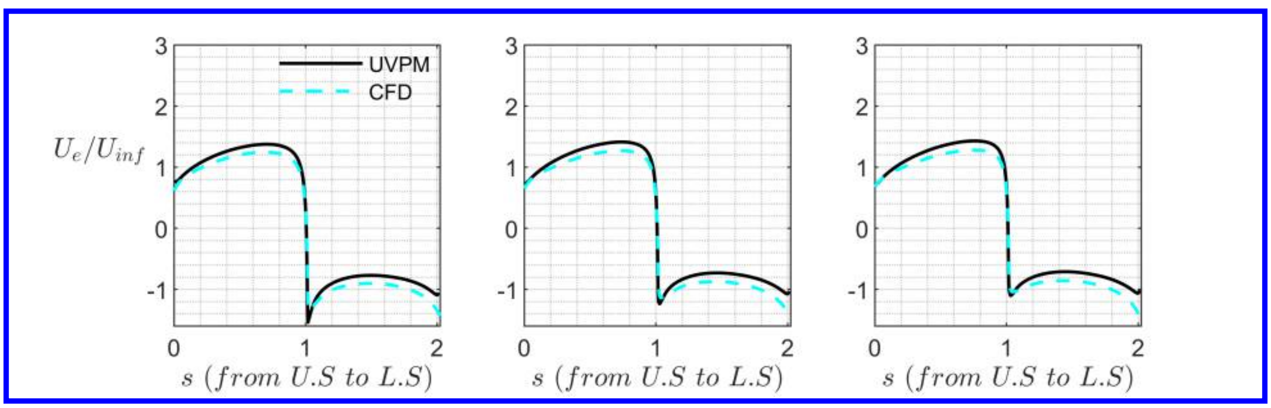

Fig. 7. Velocity distributions for K = 0.4, half-chord pivot (L-R) (a) α = 6.0° **(b)** α = 8.74° **(c)** α = 10.10°

E. Integral Boundary Layer

In this work, we have used a steady integral boundary layer (IBL) method to calculate the boundary-layer development using the velocity distribution from the unsteady panel method. In our current work, we are focused on events preceding LEV formation when the flow at the leading-edge is attached. It has been shown that the unsteady panel method is capable of predicting instantaneous pressure distribution accurately and hence this can be used as an input to the IBL which will use steady boundary layer correlations to predict the state of the boundary layer. Using a quasi-steady IBL method (rather than an unsteady boundary layer method) keeps our approach fast and computationally simple.

Earlier work by McDonald and Shamroth (1971) has shown that for many conditions of interest related to dynamic stall, unsteady boundary-layer prediction can be obtained from steady boundary-layer theory using the pressure distribution from unsteady flow. More recently, Smith and Jones (2020) have shown using scaling analysis for pitching and surging airfoils that unsteady boundary-layer effects would be negligible in predicting the onset of vortex formation for motion rates similar to those being considered in this work. Our method, currently limited to handling only laminar boundary layers, is an adaptation of that presented by Selig and Maughmer (1992). We invoke the steady boundary layer closure relations from Drela and Giles (1987) using the instantaneous velocity distribution from the UVPM as input. Using the results from UVPM and IBL, the first occurrence of reversed flow near the leading-edge region is determined by identifying the time instant when H_{32} first approaches the critical value of 1.515 in this region.

F. Cases and Motion details

Case	K	Pivot	r_{LE}
1	0.1	QC	1.0
2	0.3	QC	1.0
3	0.4	LE	1.0
4	0.4	HC	1.0
5	0.4	QC	0.5
6	0.4	QC	1.0
7	0.4	QC	1.5
8	0.4	QC	2.0

Table 1. Cases studies using the SD7003 airfoils.

For the current work, one Reynolds number, three r_{LE} configurations, three pivot locations and multiple pitch rates, were simulated using the URANS CFD code described in §A, and are listed in Table 1. All motions are of pitch-up-hold type generated using Eldredge's canonical formulation(Eldredge et al. [36], Granlund et al. [37]), shown in Figure 8.

$$\alpha = \frac{K}{a_s} \ln \left[\frac{\cosh \left(a_s \left(t^* - t_1^* \right) \right)}{\cosh \left(a_s \left(t^* - t_2^* \right) \right)} \right] + \frac{\alpha_{amp}}{2} \tag{2}$$

where a_s is the smoothing parameter from Granlund et al. [37] defined as:

$$a_s = \frac{\pi^2 K}{2\alpha_{amp}(1 - \sigma)} \tag{3}$$

and

$$t_2^* = t_1^* + \frac{\alpha_{amp}}{2K} \tag{4}$$

In these equations, t_1^* and t_2^* denote the time at the start and end of the ramp respectively. For all motions simulated in this paper, $\alpha_{amp} = 90^{\circ}$ and $a_s = 11$.

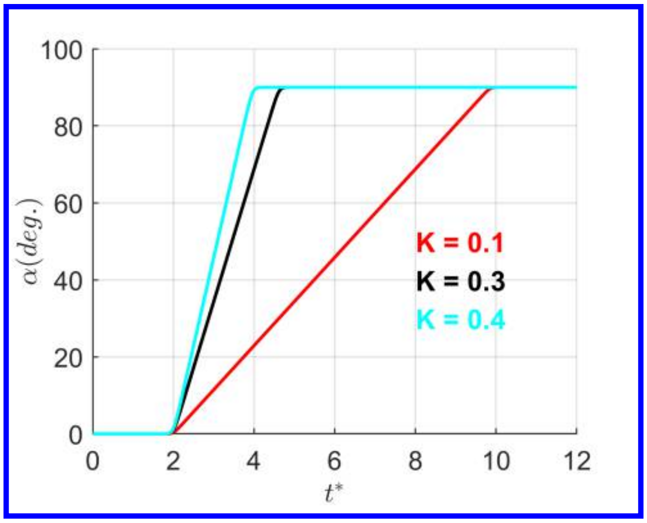

Fig. 8. Eldredge motion

The co-ordinates for different r_{LE} configurations were obtained using XFOIL(1989). All the airfoils shown in Figure 9 were generated keeping thickness and camber constant, thereby analysing variations only because of change in r_{LE}.

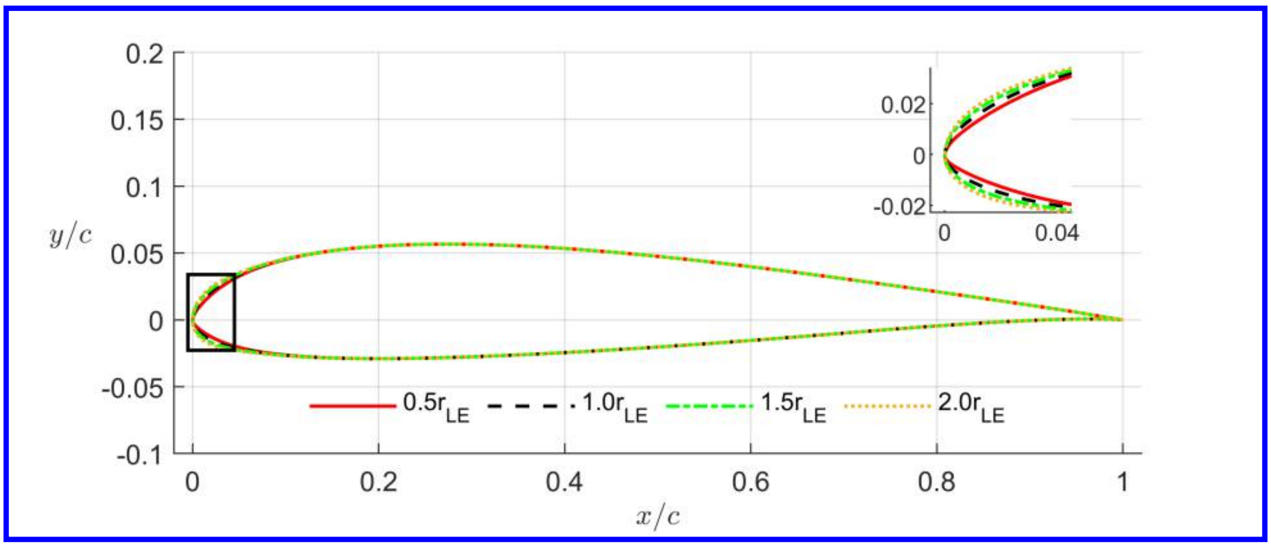

Fig. 9. SD7003 airfoil and modified variants

G. High-order prediction of LEV initiation from CFD

An important aspect is to examine the events that led to the formation of LEV for a wide range of kinematics. Although the initiation of LEV can qualitatively be inferred from the CFD flow field pictures by defining the time the first sign of LEV structure appears, it is desirable to include the approach which can be ascertained using surface quantities and be unambiguous so that the approach can be extended for any given motion. The authors have used the skin-friction (C_f) signature which is described in detail in Narsipur et al. [8]. Figure 10 displays the vorticity contours around the airfoil in each row and the corresponding C_f plots at each angle of attack. Observing the behavior of C_f plots, it can be noticed that a point of inflection occurs at $\alpha = 28.49^{\circ}$ and that signifies the onset of LEV initiation for this motion. This signature was found to be consistent for different motion kinematics and for various Reynolds numbers. More details are provided in Narsipur et al. [8] for identifying LEV initiation.

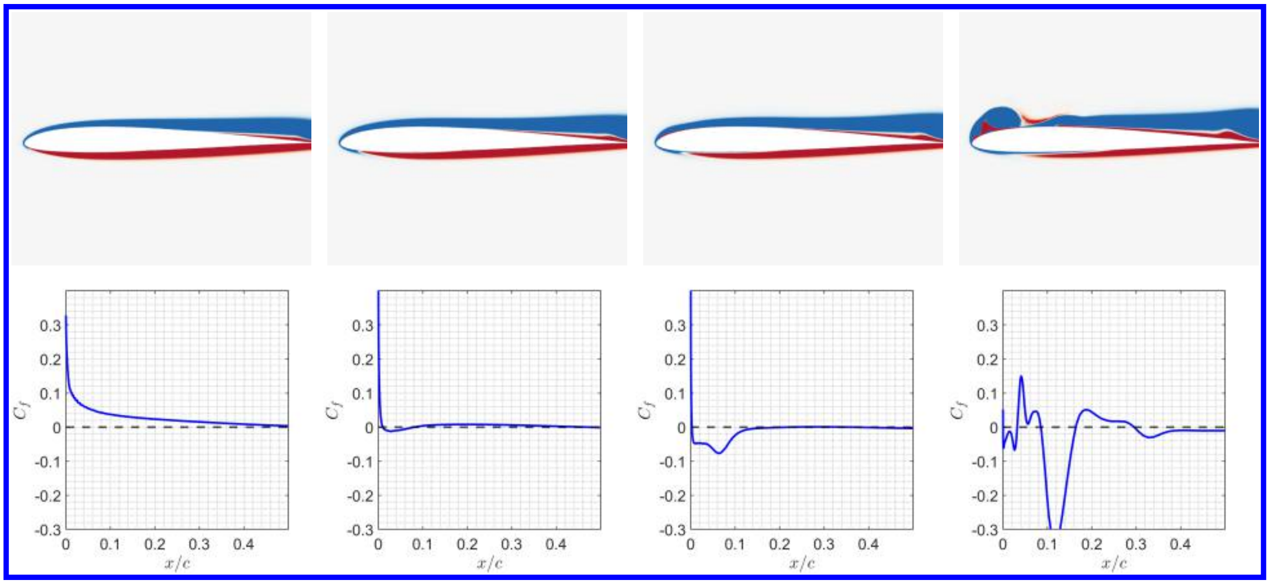

Fig. 10. LEV initiation steps (L-R) (a) α = 14.04° **(b)** α = 24.15° **(c)** α = 28.49° **(d)** α = 40.04°

H. Shape factor variation for a given motion

In this subsection, detailed results are presented for Case 6 for various values for α to illustrate the variations of flow parameters leading up to initiation of LEV formation. Figure 11 shows the upper-surface chord wise variations for C_f (left column) and H_{32} (right column) for α = 14.04, 21.26, 24.15, and 28.49 degrees (from top to bottom).

Examining the results for α = 14.04 degrees, it is seen that C_f is positive until x/c = 0.6. The H_{32} decreases from approximately 1.6 at x/c = 0 to a minimum of approximately 1.56 in the leading-edge region before finally decreasing to approximately 1.53 at x/c = 0.6. There is a small region near the trailing edge where H_{32} rises sharply and plateaus. This region is ignored in the current work because the procedure for calculation of the shape factor breaks down after flow separation. Next, examining the results for α = 21.26 degrees, it is seen that the C_f displays a similar trend near the leading-edge but the trailing edge separation location has moved upstream by a small margin ($x/c \simeq 0.5$). It is seen that the H_{32} reaches a minimum value of approximately 1.53 in the mid-chord region at this α.

The C_f plot for the final α value of 28.49 degrees has a large region of negative C_f near the leading edge. Further, it can be seen that there is a small upward spike developing in this negative-C_f region. Based on the signature described in the previous section, this occurrence in the C_f distribution consistently precedes the initiation of LEV formation in CFD results, and is taken as the critical condition corresponding to LEV initiation. Therefore, this α and the $LESP$ value from theory for this time instant are referred to as the critical values corresponding to LEV initiation. The start and end points of the negative C_f region are marked in both the C_f and H_{32} plots. For this condition, it is seen that the H_{32} decreases from approximately 2.0 to approximately 1.518 at the start of the reversed-flow region at the leading edge. This value of H_{32}, corresponding to the start of the flow-reversal region at the critical angle of attack, is denoted as the critical H_{32} value for this case (Case 6). For a portion of airfoil within the flow-reversal region, the procedure for calculation of H_{32} breaks down, resulting in artificially high values. This behavior is ignored in the current work.

For all the cases simulated as mentioned in Table 1, it was observed that H_{32} was constantly approaching a critical value $\sim$ 1.52. It is important to note that no matter where flow reversal happens on the surface of the airfoil, H_{32} at that location of reversal remains the same. Also, H_{32} at the first instance of flow reversal ($\sim$ 24.1°) and at the onset of LEV initiation ($\sim$ 28.5°) are very similar. Two major insights that can be drawn from this effort are:

1) Since we are interested in characterizing leading-edge separation, it is important to track not just the H_{32} behavior but also look at the C_f variation with (x/c) (at least from CFD).
2) There is very little difference in H_{32} values at the onset of flow reversal between the two events i.e. first occurrence of leading-edge flow reversal and the onset of LEV initiation. Hence, the low-order model can only predict the occurrence of leading-edge flow reversal with certainty, not the onset of LEV initiation.

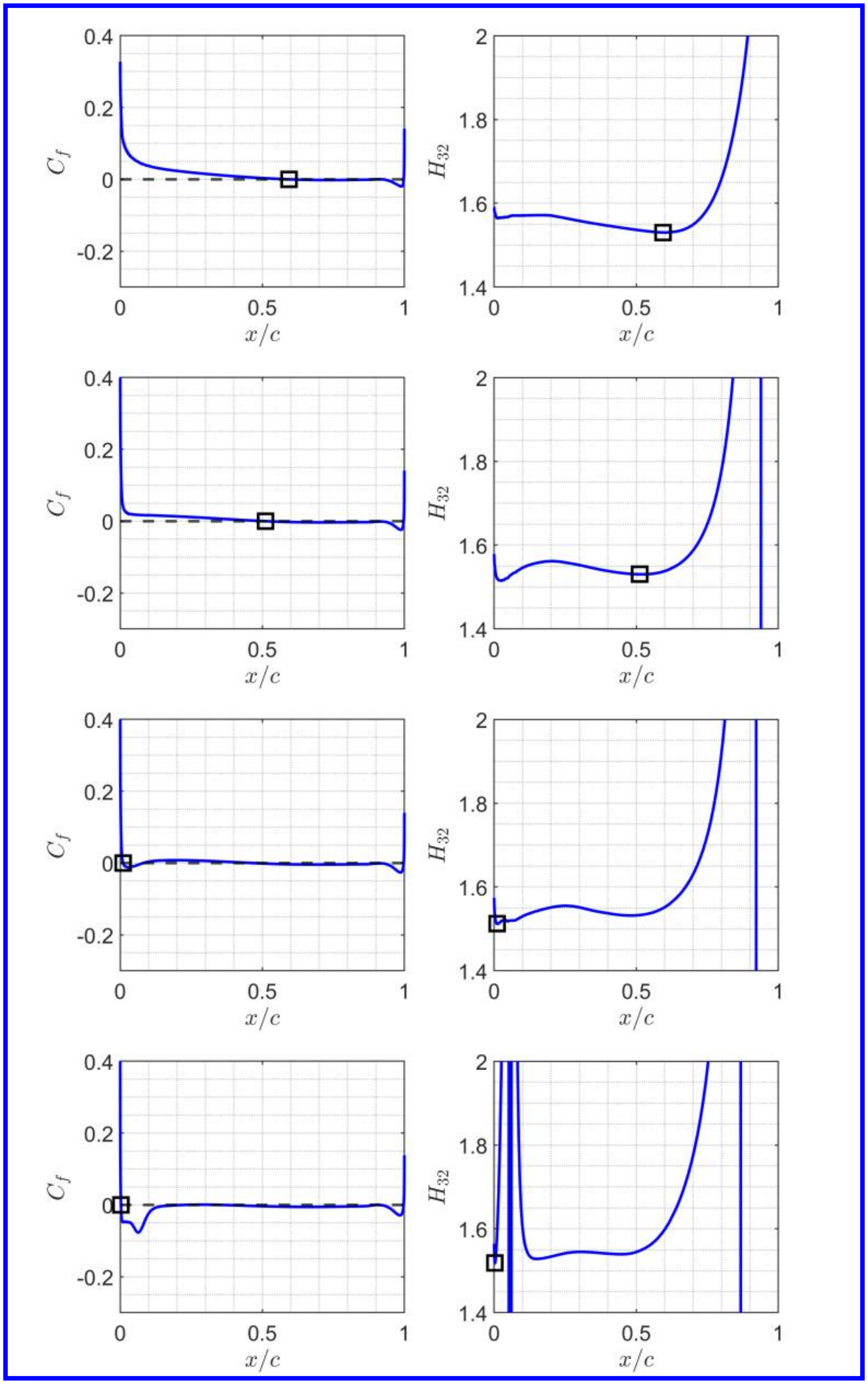

Fig. 11. C_f **and** H_{32} **variation for for** α **= 14.04, 21.26, 24.15, and 28.49 degrees (from top to bottom)**

I. Low-Order model development

In the next step, we study the variation of C_f with x/c from CFD and H_{32} with x/c from IBL. Figure 12 shows the C_f variation with x/c while Figure 13 tracks the movement of x_{sep}/c with increasing $LESP$. As discussed earlier, we are interested in identifying first occurrence of leading edge flow reversal in both IBL and CFD.

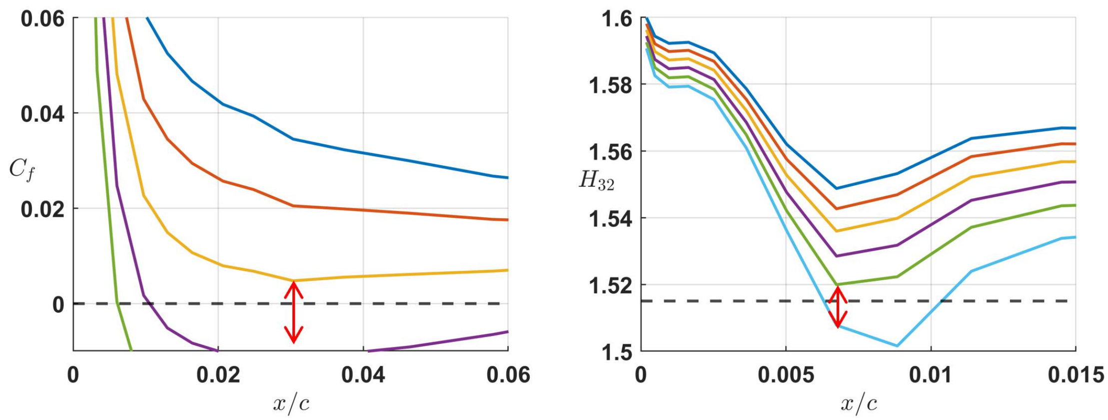

(a) C_f **v/s (x/c)** **(b)** H_{32} **v/s (x/c)**

Fig. 12. Identifying onset of reversal using a) CFD and b)IBL

It has already been demonstrated from CFD results that, at the instant of LEV initiation, H_{32} settles around 1.52 which also corresponds to the instance where C_f crosses zero indicating flow reversal. For the same motion, we've chosen instances from the analysis of IBL results where H_{32} distribution eventually settles at around 1.515, which we are using as the value corresponding to occurrence of flow reversal for the laminar boundary layer. To identify the exact angle of attack at which reversal occurs, we perform interpolation between two successive instances using C_f and H_{32} values in CFD and IBL respectively as shown by the red arrows in Figs. 12.

In addition to this, we're also interested in tracking the movement of x_{sep}/c to demarcate between trailing edge and leading edge separation. We've earmarked two such instances (red squares in Figs. 13(a) and (b)). We can notice that though the values of α predicted by UVPM and CFD might not be close ($\alpha_{IBL} = 12.84^{\circ}$ and $\alpha_{CFD} = 24.15^{\circ}$), it is interesting to see that the $LESP$ values at which the x_{sep}/c suddenly jumps forward are extremely close ($LESP_{IBL} = 0.208$ and $LESP_{CFD} = 0.239$). The instances marked in the IBL-calculated $LESP$ values are actually events corresponding to the first instance of leading edge flow reversal and not the onset of LEV initiation.

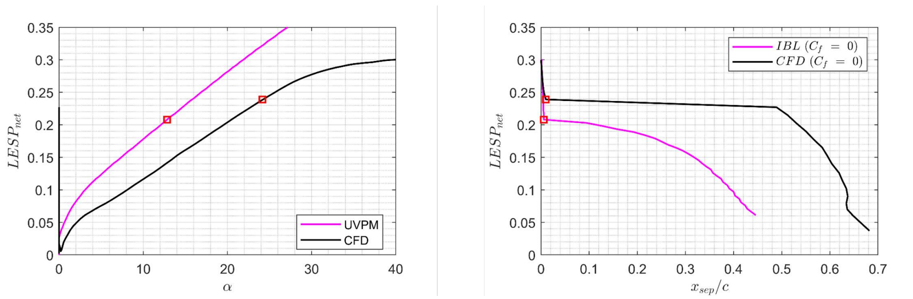

QC pivot , K = 0.4		
	α	$LESP_{net}$
IBL	12.84	0.208
CFD	24.15	0.239

(a) r_{LE} 1.0, QC pivot, K = 0.4 (baseline case)

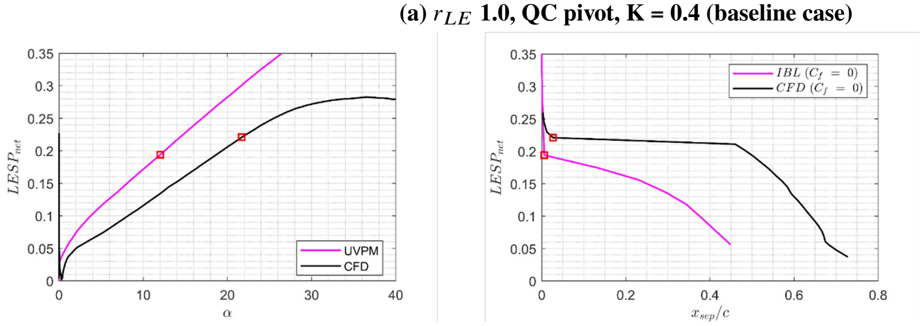

QC pivot , K = 0.3		
	α	$LESP_{net}$
IBL	12.03	0.194
CFD	21.70	0.221

(b) r_{LE} 1.0, QC pivot, K = 0.3

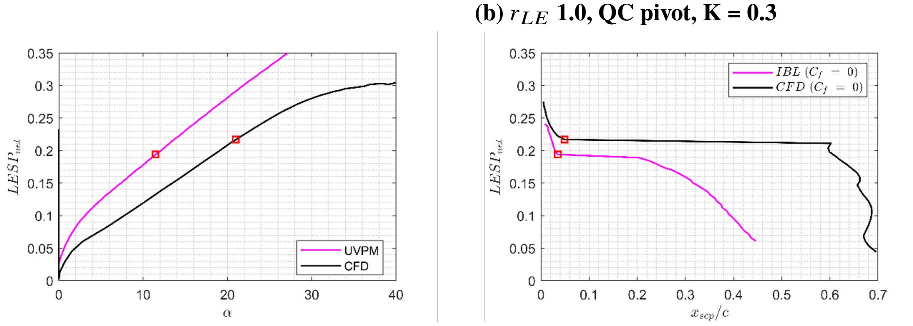

LERA 1.5 , QC pivot		
	α	$LESP_{net}$
IBL	11.47	0.194
CFD	20.98	0.217

(c) r_{LE} 1.5, QC pivot, K = 0.4

Fig. 13. LESP comparisons

IV. Results

Numerical computations were performed for SD7003 airfoil at Re 10000 for three pivot locations (x_p/c), three leading edge radii (r_{LE}) and three pitch rates (K) . We also looked at α_{onset}, $LESP$ variations along with H_{32} for the baseline case (Case 6). The filled circle represents the parameters for the baseline case (K = 0.4, r_{LE} = 1.0 and QC pivot).

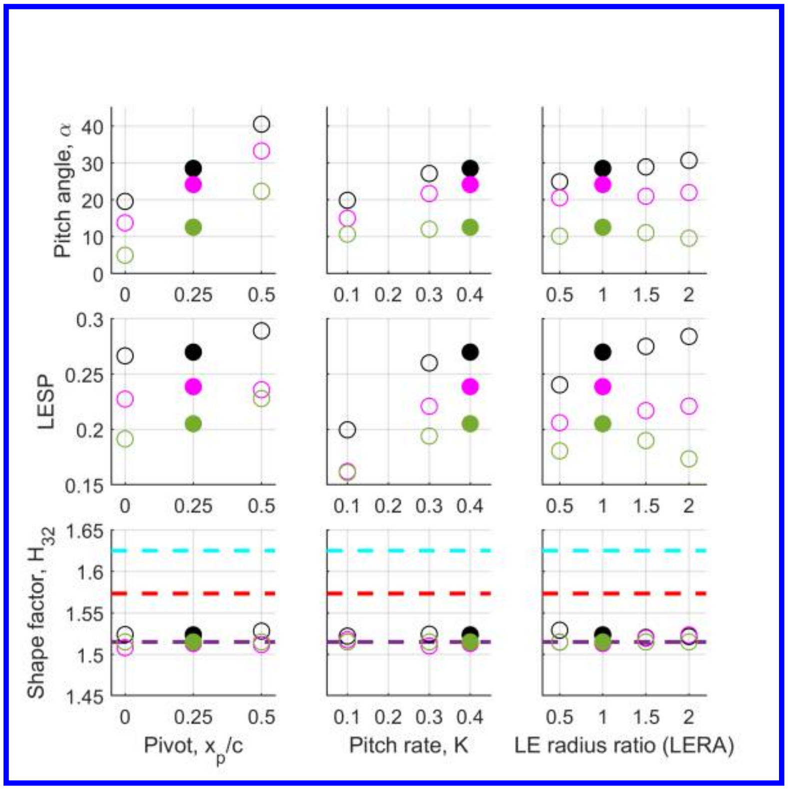

Fig. 14. Scatter plots for critical values of α_{onset}, $LESP_{onset}$ and H_{32}. Symbols: onset of LEV initiation in CFD (black), first onset of flow reversal in CFD (pink) and first onset of flow reversal in IBL (green).

We have co-plotted results for pitch-up motions in Figure 14 from CFD and IBL at three instances: onset of LEV initiation in CFD (black), first onset of flow reversal in CFD (pink) and first onset of flow reversal in IBL (green). Looking at the pivot-location effects (column 1) first, it is understandable that α_{onset} increases as the pivot location is changed from leading edge to half chord due to the effect of the increased motion-induced downwash at the leading edge as pivot is moved aft. LESP is known to be independent of pivot location and hence we see it being almost constant across the three pivots. Meanwhile, H_{32} from both CFD and IBL are seen to be a near-constant value of 1.52. Also shown as dashed lines for reference are the H_{32} values (for steady, incompressible flow) of 1.515 (purple) corresponding to laminar separation, 1.57 (red) corresponding to a flat plate zero pressure gradient (ZPG) flow and 1.62 (cyan) corresponding to stagnation-point flow.

In the next parameter set (column 2) we look at variations with pitch rate (K). It is seen that α_{onset} increases with pitch rate. Higher pitch rate delays flow separation at the leading edge due to higher motion-induced downwash. It is seen that LESP shows some dependence on pitch rate (noted by [39] and [40]). The reason for this behavior is not clear at this time. Finally, it is seen that the H_{32} values for all cases occur close to the value of 1.52.

In the final parameter study (column 3), we looked at variations with r_{LE}. It is seen that α_{onset} initially increases and then decreases with r_{LE}. A similar behavior is seen for the trend in $LESP$ variation with r_{LE}. However, H_{32}, as in earlier observations, continues to be close to the value of 1.52 across all r_{LE} values.

V. Conclusions

The current work has focused on two specific areas : identification of a new boundary-layer parameter (H_{32}) that shows criticality in the event of an LEV formation and then implementing this parameter to develop a low-order model that identifies the LESP at which first occurrence of leading-edge flow reversal is observed. Though LESP has been the most convincing criterion amongst numerous efforts to characterize LEV initiation, its applicability in a low order model is hindered by its dependence on Re and r_{LE}. In this work, a series of computational studies were carried to investigate the boundary layer behavior in the vicinity of the leading-edge to unearth H_{32} as a novel criterion. The computational studies spanned parametric variations in leading-edge radius ratio (r_{LE}) and pitch rate (K), factors that are attributed for $LESP$ variation.

For all the cases observed, it was observed that H_{32} attains a critical value of 1.52 near the instant of LEV formation. This was achieved irrespective of the change in leading edge radius (r_{LE}) from 0.5 to 2.0. The results presented here provide verification for boundary-layer criticality being the cause for the first occurrence of flow reversal at the leading edge. This flow condition is a precursor to initiation of LEV formation. The approach presented here uses this insight in the development of a low-order approach to predict occurrence of leading-edge flow reversal without the use of CFD. Although the IBL method cannot be applied beyond the first occurrence of flow reversal, the difference in LESP between first flow reversal and LEV initiation is roughly the same for all motions studied thus far. This means the current approach can be successfully used to estimate LEV initiation for any airfoil and motion combination. In a nutshell, we intend on using this predictive tool to identify the equivalent $LESP$, i.e. the instance at which $LESP_{inviscid} = LESP_{viscous}$ instead of identifying the pitch angle at which reversal would start. We believe that the current work provides a path for determining the critical LESP without the use of CFD.

References

[1] Muijres, F. T., Johansson, L. C., Barfield, R., Wolf, M., Spedding, G. R., and Hedenström, A., "Leading-Edge Vortex Improves Lift in Slow-Flying Bats," *Science*, Vol. 319, No. 5867, 2008, pp. 1250–1253.

[2] Ham, N. D., and Garelick, M. S., "Dynamic Stall Considerations in Helicopter Rotors," *Journal of the American Helicopter Society*, Vol. 13, 1968, pp. 49–55.

[3] Su, Y., and Breuer, K., "Resonant response and optimal energy harvesting of an elastically mounted pitching and heaving hydrofoil," *Physical Review Fluids*, Vol. 4, No. 6, 2019, p. 064701.

[4] Evans, W. T., and Mort, K. W., *Analysis of computed flow parameters for a set of sudden stalls in low-speed two-dimensional flow*, Vol. 85, National Aeronautics and Space Administration, 1959.

[5] Baik, Y. S., Bernal, L. P., Granlund, K., and Ol, M. V., "Unsteady force generation and vortex dynamics of pitching and plunging aerofoils," *Journal of Fluid Mechanics*, Vol. 709, 2012, pp. 37–68.

[6] Ramesh, K., Gopalarathnam, A., Granlund, K., Ol, M. V., and Edwards, J. R., "Discrete-vortex method with novel shedding criterion for unsteady airfoil flows with intermittent leading-edge vortex shedding," *Journal of Fluid Mechanics*, Vol. 751, 2014, pp. 500–538. doi:10.1017/jfm.2014.297.

[7] Wang, C., and Eldredge, J. D., "Low-order phenomenological modeling of leading-edge vortex formation," *Theor. Comput. Fluid Dyn.*, Vol. 27, No. 5, 2013, pp. 577–598.

[8] Narsipur, S., Hosangadi, P., Gopalarathnam, A., and Edwards, J. R., "Variation of leading-edge suction during stall for unsteady aerofoil motions," *Journal of Fluid Mechanics*, Vol. 900, 2020.

[9] Carr, L., Carr, K., and McCroskey, W., "Analysis of the development of dynamic stall based on oscillation airfoil experiments." *NASA Technical Note TN D-8382*, 1977.

[10] McCroskey, W. J., "Unsteady Airfoils," *Annu. Rev. Fluid Mech.*, Vol. 14, No. 1, 1982, pp. 285–311.

[11] Prandtl, L., "Über Flussigkeitsbewegung bei sehr kleiner Reibung," *Verhandl. III, Internat. Math.-Kong., Heidelberg, Teubner, Leipzig, 1904*, 1904, pp. 484–491.

[12] Haller, G., "Exact theory of unsteady separation for two-dimensional flows," *Journal of Fluid Mechanics*, Vol. 512, 2004, pp. 257–311.

[13] Klose, B. F., Jacobs, G. B., and Serra, M., "Kinematics of Lagrangian flow separation in external aerodynamics," *AIAA Journal*, Vol. 58, No. 5, 2020, pp. 1926–1938.

[14] Acharya, M., and Metwally, M. H., "Unsteady Pressure Field and Vorticity Production over a Pitching Airfoil," *AIAA Journal*, Vol. 30, No. 2, 1992, pp. 403–411.

[15] Gehlert, P., and Babinsky, H., "Boundary layer vortex sheet evolution around an accelerating and rotating cylinder," *Journal of Fluid Mechanics*, Vol. 915, 2021.

[16] Gendrich, C. P., "Dynamic stall of rapidly pitching airfoils: MTV experiments and Navier-Stokes simulations," Ph.D. thesis, Michigan State University, 1999.

[17] Smith, L. R., and Jones, A. R., "Vortex formation on a pitching aerofoil at high surging amplitudes," *J. Fluid Mech.*, Vol. 905, 2020, p. A22.

[18] Schlichting, H., and Gersten, K., *Boundary-layer theory*, Springer Science & Business Media, 2003.

[19] Erturk, E., Haddad, O. M., and Corke, T. C., "Laminar Incompressible Flow Past Parabolic Bodies at Angles of Attack," *AIAA Journal*, Vol. 42, No. 11, 2004, pp. 2254–2265. doi:10.2514/1.4032, URL `http://arc.aiaa.org/doi/10.2514/1.4032`.

[20] Castillo, L., Wang, X., and George, W. K., "Separation criterion for turbulent boundary layers via similarity analysis," *J. Fluids Eng.*, Vol. 126, No. 3, 2004, pp. 297–304.

[21] Ramanathan, H., Narsipur, S., and Gopalarathnam, A., "Boundary-Layer Characteristics at the Onset of Leading-Edge Vortex Formation on Unsteady Airfoils," *AIAA Aviation 2019 Forum*, 2019, p. 3590.

[22] Beddoes, T., "Onset of leading edge separation effects under dynamic conditions and low Mach number," *American Helicopter Society, Annual National Forum, 34 th, Washington, D. C, Proceedings, Research supported by the Ministry of Defence,(Procurement Executive)*, Vol. 15, 1978.

[23] Katz, J., "A Discrete Vortex Method for the Non-Steady Separated Flow over an Airfoil," *Journal of Fluid Mechanics*, Vol. 102, 1981, pp. 315–328.

[24] Fulton, J., Edwards, J., Hassan, H., Rockwell, R., Goyne, C., McDaniel, J., Smith, C., Cutler, A., Johansen, C., Danehy, P., et al., "Large-eddy/Reynolds-averaged Navier-Stokes simulation of a dual-mode scramjet combustor," *50th AIAA aerospace sciences meeting including the new horizons forum and aerospace exposition*, 2012, p. 115.

[25] Edwards, J. R., "Simulation of transient dynamics of shock wave boundary layer interactions using hybrid Large-eddy/Reynolds-averaged Navier-Stokes models," Tech. rep., NORTH CAROLINA STATE UNIV AT RALEIGH, 2007.

[26] Cassidy, D. A., Edwards, J. R., and Tian, M., "An Investigation of Interface-Sharpening Schemes for Multiphase Mixture Flows," *Journal of Computational Physics*, Vol. 228, No. 16, 2009, pp. 5628–5649.

[27] Colella, P., and Woodward, P. R., "The Piecewise Parabolic Method (PPM) for Gas-dynamic Simulations," *Journal of Computational Physics*, Vol. 54, 1984, pp. 174–201.

[28] Edwards, J. R., and Chandra, S., "Comparison of Eddy Viscosity-Transport Turbulence Models for Three-Dimensional, Shock-Separated Flowfields," *AIAA Journal*, Vol. 34, No. 4, 1996, pp. 756–763.

[29] Lee, T., and Gerontakos, P., "Investigation of flow over an oscillating airfoil," *J. Fluid Mech.*, Vol. 512, 2004.

[30] Hess, J., and Smith, A., "Calculation of potential flow about arbitrary bodies," *Progress in Aerospace Sciences*, Vol. 8, 1967, pp. 1–138.

[31] Katz, J., and Plotkin, A., *Low-speed aerodynamics*, Vol. 13, Cambridge university press, 2001.

[32] Müller-Vahl, H. F., Strangfeld, C., Nayeri, C. N., Paschereit, C. O., and Greenblatt, D., "Control of thick airfoil, deep dynamic stall using steady blowing," *AIAA journal*, Vol. 53, No. 2, 2015, pp. 277–295. URL `https://www.flowcontrollab.com/data-resource`.

[33] Mcdonald, H., and Shamroth, S. J., "An analysis and application of the time- dependent turbulent boundary-layer equations," *AIAA Journal*, Vol. 9, No. 8, 1971, pp. 1553–1560. doi:10.2514/3.6391, URL `https://arc.aiaa.org/doi/10.2514/3.6391`.

[34] Selig, M. S., and Maughmer, M. D., "Generalized multipoint inverse airfoil design," *AIAA journal*, Vol. 30, No. 11, 1992, pp. 2618–2625.

[35] Drela, M., and Gilest, M. B., "Viscous-Inviscid Analysis of Transonic and Low Reynolds Number Airfoils," *AIAA JOURNAL*, 1987, p. 9.

[36] Eldredge, J., Wang, C., and Ol, M., "A computational study of a canonical pitch-up, pitch-down wing maneuver," *39th AIAA fluid dynamics conference*, 2009, p. 3687.

[37] Granlund, K. O., Ol, M. V., and Bernal, L. P., "Unsteady pitching flat plates," *J. Fluid Mech.*, Vol. 733, 2013, p. R5.

[38] Drela, M., "XFOIL: An analysis and design system for low Reynolds number airfoils," *Low Reynolds number aerodynamics*, Springer, 1989, pp. 1–12.

[39] Deparday, J., and Mulleners, K., "Critical evolution of leading edge suction during dynamic stall," *J. Phys.: Conf. Ser.*, Vol. 1037, 2018, p. 022017.

[40] Kay, N. J., Richards, P. J., and Sharma, R. N., "Low-Reynolds Number Behavior of the Leading-Edge Suction Parameter at Low Pitch Rates," *AIAA Journal*, 2021, pp. 1–9. doi:10.2514/1.J060733, URL `https://arc.aiaa.org/doi/10.2514/1.J060733`.